


Origin of spectral topology in non-Hermitian Aubry-André-Harper models

Xiaoming Cai ^{*}

Innovation Academy for Precision Measurement Science and Technology, Chinese Academy of Sciences, Wuhan 430071, China



(Received 28 November 2024; accepted 18 February 2025; published 5 March 2025)

We investigate localization and topological properties of a non-Hermitian generalization of the Aubry-André-Harper (AAH) model, which is the dimension reduction of the two-dimensional non-Hermitian quantum Hall model. Non-Hermiticity arises from the nonreciprocal hopping and the complex global phase. In the absence of nonreciprocal hopping, by applying Avila's global theory we analytically compute the localization length of states and determine phase diagrams. The complex global phase is in favor of the critical phase, whose transition to the localized phase falls outside the universality class of the classic AAH model. By mapping to the Hall model, we further demonstrate that the loop structure in spectrum originates from the spectral topology in the reduced dimension. When the nonreciprocal hopping is added, the localization is analytically studied by employing a similarity transformation, and phase diagrams are determined exactly. The system has boundary-dependent spectra and states because of the nontrivial spectral topology in the remaining physical dimension. The critical phase no longer exists, and the nonreciprocal hopping favors the extended phase when under the periodic boundary condition. Loops always exist in the complex spectrum but have distinct topological origins in different phases.

DOI: [10.1103/PhysRevB.111.125109](https://doi.org/10.1103/PhysRevB.111.125109)

I. INTRODUCTION

The Aubry-André-Harper (AAH) model is one of the main tools for studying quantum localization and topological states of matter in one dimension (1D) [1,2]. It is produced when the 2D quantum Hall model is reduced to a 1D chain [2,3]. It displays topological characteristics, including Thouless pumping and a well-defined bulk topological invariant [4–6]. When made quasiperiodic, the AAH model undergoes a sharp metal-insulator transition at a threshold quasiperiodic potential strength [2,3,7], whereas the localization of states happens for an infinitesimal random disorder [8]. In recent years, a wealth of unique scenarios in the context of localization and topological transitions have been produced via generalizations of the AAH model [9–20]. A significant example of these extensions is produced by introducing quasiperiodic modulations on off-diagonal hoppings [21–24]. The model, which is exactly solvable, supports a critical phase, and states in the phase exhibit self-similarity and fractal dimensions. Various artificial systems have been used to experimentally realize the AAH models, including those that support the critical phase [4,25–31].

On the other hand, the study of fascinating properties and applications of non-Hermitian systems has recently attracted increasing attention [32–40]. Non-Hermiticity arises via exchanges of energy and/or particles with the environment and is expressed in the Hamiltonian through the introduction of nonreciprocal hoppings and/or complex potentials. It gives rise to a number of exotic phenomena, including parity-time (\mathcal{PT}) symmetry breaking [41,42], non-Hermitian topology [43,44], skin effect [45,46], and revised bulk-edge

correspondence [47–52]. In particular, the presence of skin effect under the open boundary condition (OBC), i.e., the accumulation of an extensive number of eigenstates at the edges, is in accordance with the nontrivial spectral topology under the periodic boundary condition (PBC) [46]. Non-Hermitian generalizations of the AAH model also have been extensively investigated [53–84], especially stimulated by recent experimental studies of their intriguing topological and transport properties [85,86]. Boundary-dependent state topologies, self-dualities, and asymmetrical localization arise from the interplay of nonreciprocal hopping and (quasi)periodicity [55,63,70,87,88]. Complex quasiperiodic potentials lead to unconventional \mathcal{PT} symmetry breaking [56–59,62], butterfly spectra [57,63], topological edge states [59–63], spectral topologies [61], mobility edges [73,87,89–91], and modified localizations [54,62–68,88]. Particularly, it was reported that the localization transition is accompanied by the change of spectral topology when the strength of complex quasiperiodic potential increases [61]. However, the physical origin of the spectral topology has not yet been pointed out. Moreover, skin states are absent under the OBC despite the presence of nontrivial spectral topology, which is inconsistent with the correspondence mentioned above and deserves a detailed explanation. In addition, despite the fact that extensive studies have been done on AAH models, the exactly solvable ones with analytical localization properties are few, especially rare for those with off-diagonal modulations [79,92]. The localization and topological properties of non-Hermitian generalizations with both on-site and off-diagonal modulations, as well as the fate of the critical phase against non-Hermiticity, are largely unexplored [72].

In this paper, we study localization and topological properties of generalized AAH models with both on-site and off-diagonal quasiperiodic modulations. Non-Hermiticity

^{*}Contact author: cxmpx@wipm.ac.cn

arises from the nonreciprocal hopping and the complex phase. By mapping to the 2D non-Hermitian quantum Hall models, we explain physical origins of spectral topologies in AAH models, their relations to the topologies in different dimensions of the 2D model, and the discordance between spectral topology and the skin effect. Through this mapping, we further explain why the duality transformation for the classic AAH model does not work for non-Hermitian ones. Localization properties are analytically obtained in a two-step calculation. In the absence of nonreciprocal hopping, we analytically compute the localization length of single-particle states by applying Avila's global theory of one-frequency Schrödinger operators [93]. After introducing the nonreciprocal hopping, the localization is analytically studied by employing a similarity transformation. The model suffers from the non-Hermitian skin effect, which results in boundary-dependent and asymmetrical localization. We determine localization phase diagrams and analyze the fate of critical phase and effects of the non-Hermiticity on the localization. \mathcal{PT} symmetry breaking (or real-complex transition) and topological phase transition of the spectrum are also numerically studied, which are partially in accordance with the localization phase transition.

The remainder of the paper is arranged as follows. In Sec. II, we introduce non-Hermitian generalized AAH models and the related 2D non-Hermitian quantum Hall models. Section III is devoted to the study of the situation without nonreciprocal hopping. We analytically compute the localization length and examine localization properties. The real-complex transition and the spectral topology are also numerically investigated. The origin of spectral topology and the fate of the critical phase are also discussed in the process. In Sec. IV, we analytically study the asymmetrical localization, brought about by the nonreciprocal hopping. Additionally analyzed are boundary-dependent properties, such as the critical phase, skin phase, real-complex transition, spectral topology, and origin of it. Ultimately, we conclude our primary findings in Sec. V.

II. MODEL AND HAMILTONIAN

The generalized AAH model under consideration is described by the following tight-binding Hamiltonian,

$$H = \sum_j [t_j(e^{-\eta}c_j^\dagger c_{j+1} + e^\eta c_{j+1}^\dagger c_j) + V_j c_j^\dagger c_j]. \quad (1)$$

c_j^\dagger (c_j) is the operator that creates (annihilates) a spinless particle at site j ; η characterizes the nonreciprocity of hoppings and is responsible for the non-Hermitian skin effect [45]; t_j and V_j are the incommensurately modulated hopping amplitude and on-site potential, respectively, which are provided by

$$\begin{aligned} t_j &= t + W \cos[2\pi\beta(j + 1/2) + \theta - ih], \\ V_j &= 2V \cos(2\pi\beta j + \theta - ih + \delta); \end{aligned} \quad (2)$$

and t is the unmodulated part of hopping amplitude and establishes the unit of energy ($t = 1$). W and V represent the modulation amplitudes of the off-diagonal hopping and on-site potential, respectively. $\theta - ih$ is the complex global phase, which is the second source of non-Hermiticity. Its

real part θ is insignificant in the localization, and we shall assign $\theta = 0$ if not supplied. An adjustable relative phase δ between on-site and off-diagonal modulations, on which the localization and topological properties of the model critically depend, is also introduced [23]. In the presence of phases θ and δ , both W and V can be set to positive real numbers. β is an irrational number that characterizes the quasiperiodicity of modulations. The modulations are incommensurate with respect to the underlying lattice, act as quasirandom disorders, and result in the localization of states. We take the value of golden ratio $[\beta = (\sqrt{5} - 1)/2]$ as usual, and in numerical calculations it is approximated by rational numbers $\beta = F_n/F_{n+1}$, where F_n is the n th Fibonacci number. Correspondingly, the total number of lattice sites is chosen as $L = F_{n+1}$.

When $\eta = h = 0$, the model becomes the Hermitian one discussed in Ref. [23], where phase diagrams on localization have been analytically determined by bandwidth computation. The system sustains a sizable critical phase when $W > t$, $V < W$, and $\delta = 0$. When $\eta = W = 0$, the model reverts to the non-Hermitian one explored in Ref. [61], where only the on-site quasiperiodic modulation exists. It was demonstrated that the critical quasiperiodic potential strength is the same for \mathcal{PT} symmetry breaking, topological phase transition, and localization phase transition. When $W = 0$, the interplay between the non-Hermitian skin effect and localization was examined in Ref. [53], leading to boundary-dependent \mathcal{PT} symmetry breaking, spectral topology, and asymmetrical localization.

It is well known that the classic AAH model is the dimension reduction of the 2D quantum Hall model, describing particles hopping on the square lattice threaded by a homogeneous magnetic field. The 2D model corresponding to Eq. (1) is described by the following Hamiltonian:

$$\begin{aligned} H_{2D} &= \sum_{m,n} t e^\eta c_{n+1,m}^\dagger c_{n,m} + t e^{-\eta} c_{n,m}^\dagger c_{n+1,m} \\ &+ V e^{i(2\pi\beta n + \delta) + h} c_{n,m+1}^\dagger c_{n,m} \\ &+ V e^{-i(2\pi\beta n + \delta) - h} c_{n,m}^\dagger c_{n,m+1} \\ &+ \frac{W}{2} e^{i2\pi\beta(n + \frac{1}{2}) + \eta + h} c_{n+1,m+1}^\dagger c_{n,m} \\ &+ \frac{W}{2} e^{-i2\pi\beta(n + \frac{1}{2}) - \eta - h} c_{n,m}^\dagger c_{n+1,m+1} \\ &+ \frac{W}{2} e^{-i2\pi\beta(n + \frac{1}{2}) + \eta - h} c_{n+1,m}^\dagger c_{n,m+1} \\ &+ \frac{W}{2} e^{i2\pi\beta(n + \frac{1}{2}) - \eta + h} c_{n,m+1}^\dagger c_{n+1,m}, \end{aligned} \quad (3)$$

where $c_{n,m}^\dagger$ is the creation operator at the lattice site (n, m) and n and m are indexes of sites in the x and y dimensions, respectively. Terms in the first line describe hoppings in the x dimension with t the geometric average of hopping amplitudes and η characterizing the nonreciprocity (see also in Fig. 1). V , which is the strength of complex quasiperiodic potential in the 1D AAH model, is the geometric average of hopping amplitudes in the y dimension, and h characterizes the nonreciprocity in this direction. W is the geometric average of next-nearest-neighbor hopping amplitudes, which experience nonreciprocities in both x and y dimensions.

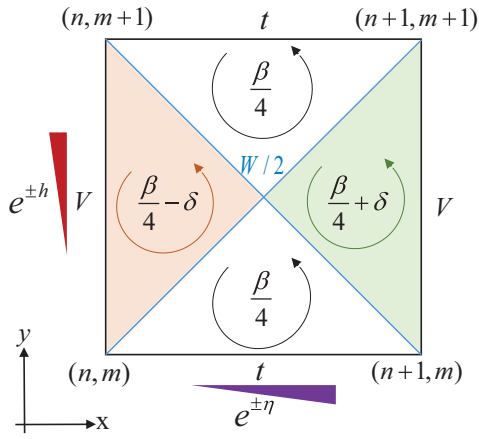


FIG. 1. Unit cell of the 2D non-Hermitian quantum Hall model which gives rise to the generalized AAH model.

β characterizes the strength of the uniform magnetic field with β flux quanta per unit cell, and the magnetic vector potential is given by the Landau gauge $A_y = \beta n$. The relative phase δ requires that the 2D model has a nonuniform magnetic flux, with the left and right quadrants of each unit cell receiving extra $\pm\delta$ flux, respectively, as shown in Fig. 1. The 2D model has translational symmetry in the y dimension where the PBC is employed. Then, after performing the Fourier transformation in the y dimension, we obtain the dimension reduction, which is precisely the model shown in Eq. (1). The global phase θ plays the role of momentum in the y dimension. Please refer to Appendix A for more details. On the other hand, we can also employ another gauge $A_x = -\beta m$, and the 2D model has translational symmetry in the x dimension. After performing the Fourier transformation in the x dimension, we obtain a reduced model which is similar to Eq. (1). When $\delta = 0$, it is in the same form as Eq. (1), but with simultaneous interchanges $t \leftrightarrow V$ and $\eta \leftrightarrow h$ and an additional conjugation. These two reduced non-Hermitian AAH models are related by the duality transformation for the classic AAH model. The presence of conjugation makes the non-Hermitian AAH models not self-dual through the traditional duality transformation. The model in Eq. (1) supports the duality transformation introduced in Ref. [53].

III. LOCALIZATION AND TOPOLOGY IN THE ABSENCE OF NONRECIPROCAL HOPPING ($\eta = 0$)

The model in Eq. (1) includes two sources of non-Hermiticity, and to clearly explore the physical features we

will proceed in two phases. This section is devoted to the situation that non-Hermiticity is limited to the imaginary phase ih . Then, in the following section, we incorporate the nonreciprocity η , which is the source of the skin effect and causes boundary-dependent behaviors.

When the nonreciprocity of hopping is absent, we analytically compute the Lyapunov exponent (LE) (or inverse of localization length) of eigenstates, by using Avila's global theory of one-frequency analytical $SL(2, \mathbb{C})$ cocycle [93]. For a single-particle state $|\Phi\rangle = \sum_j \phi_j c_j^\dagger |0\rangle$ with eigenenergy E , the transfer matrix version of the Schrödinger equation of amplitudes ϕ_j is

$$\begin{bmatrix} \phi_{j+1} \\ \phi_j \end{bmatrix} = T_j \begin{bmatrix} \phi_j \\ \phi_{j-1} \end{bmatrix}, \quad T_j = \begin{bmatrix} \frac{E-V_j}{t_j} & -\frac{t_{j-1}}{t_j} \\ 1 & 0 \end{bmatrix}. \quad (4)$$

The LE of the state is computed by

$$\begin{aligned} \gamma &= \lim_{L \rightarrow \infty} \frac{1}{L} \ln \left\| \prod_{j=1}^L T_j \right\|, \\ &= \begin{cases} \max(f_1, 0), & W \leq t / \cosh(h), \\ \max(f_2, 0), & W > t / \cosh(h), \end{cases} \end{aligned} \quad (5)$$

where $\|\cdot\|$ represents the norm of a matrix and

$$f_1 = |g| + \ln \frac{|Ve^{i\delta} + \sqrt{[Ve^{i\delta}]^2 - W^2}|}{t + \sqrt{t^2 - W^2}}, \quad (6)$$

$$f_2 = \ln \frac{|Ve^{i\delta} + \sqrt{[Ve^{i\delta}]^2 - W^2}|}{W}. \quad (7)$$

For a comprehensive computation, please refer to the Appendix B. Not only is the LE a periodic function of the relative phase δ with a period π , but it is also symmetric about $\delta = m\pi/2, m \in \mathbb{Z}$. Above, we have limited $\delta \in [0, \pi/2]$. Conditions $f_{1(2)} = 0$, which indicate that the state changes from extended or critical to localized, or the LE changes from $\gamma = 0$ to $\gamma > 0$, specify the localization phase transition points. $f_1 = 0$ yields

$$V^2 \left[\frac{\cos^2 \delta}{(t \cosh |h| - \sqrt{t^2 - W^2} \sinh |h|)^2} + \frac{\sin^2 \delta}{(t \sinh |h| - \sqrt{t^2 - W^2} \cosh |h|)^2} \right] = 1, \quad \text{when } W \leq t / \cosh(h), \quad (8)$$

whereas $f_2 = 0$ yields

$$V = \begin{cases} W, & \text{if } \delta = 0, \\ 0, & \text{if } \delta \neq 0, \end{cases} \quad \text{when } W > t / \cosh(h). \quad (9)$$

The LE and phase transition conditions are energy independent. Furthermore, they are independent of the irrational frequency β and the global phase θ . It is also worth noticing that $f_2 = 0$ holds in a sizable area of the parameter space,

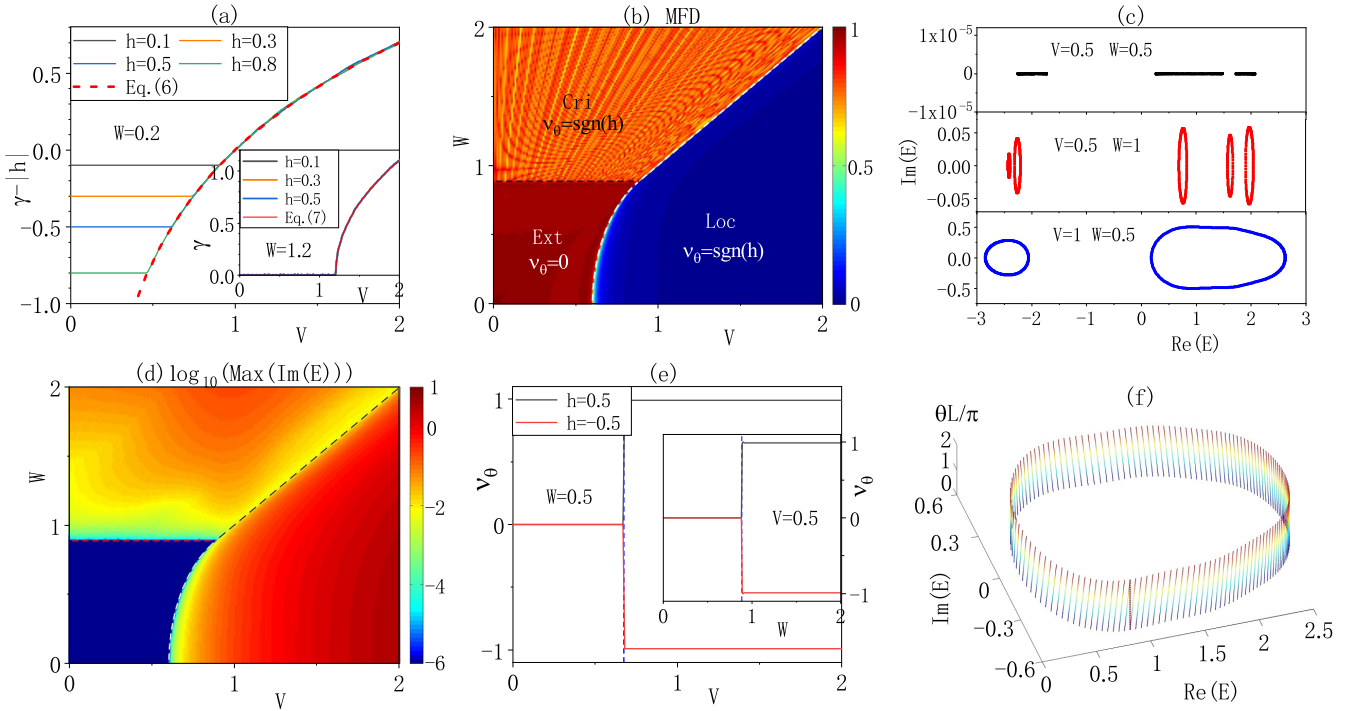


FIG. 2. Generalized AAH model in the absence of nonreciprocal hopping ($\eta = 0$), with the relative phase $\delta = 0$, and under the periodic boundary condition. In (a) and its inset we present mean LEs versus V for systems with different W . (b) Mean fractal dimension on the (V, W) plane for the system with $h = 0.5$. (c) Spectra on the complex energy plane for systems with $h = 0.5$. (d) Logarithm of the largest value of imaginary parts of all eigenenergies, as a function of V and W , for the system with $h = 0.5$. In (e) and its inset, we show the winding number ν_θ against V and W , respectively. In (f) we present how the right loop in the last panel of (c) spins as θ increases from 0 to $2\pi/L$. The system corresponding to (f) is in the localized phase and a vertical red line is added to guide the eye. The size of lattice is $L = 610$ in (a)–(e) and $L = 233$ in (f).

suggesting the existence of a critical phase when $W > t/\cosh(h)$, $V < W$, and $\delta = 0$. In addition, when $W > t/\cosh(h)$, the exact expression of LE and the conditions for phase transition are independent of h . It is evident from the above equations that the situation $\delta = 0$ is special, which we shall address separately.

A. Case $\delta = 0$

Simplified from the above equations, the localization transition occurs at the critical strength of quasiperiodic potential,

$$V_c = \max(t \cosh(h) - \sqrt{t^2 - W^2} \sinh|h|, W). \quad (10)$$

When $V > V_c$, the quasiperiodic potential dominates, and all single-particle states are localized with energy-independent LEs $\gamma > 0$, indicating that the system is in the localized phase [see Fig. 2(b)]. However, $f_1 < 0$, $\gamma = 0$, all states are extended, and the system is in the extended phase when $V < V_c$ and $W < t/\cosh(h)$. The unmodulated part of hopping prevails when the system is in the extended phase. Nevertheless, when $V < W$ and $W > t/\cosh(h)$, the quasiperiodic hopping dominates, $f_2 = 0$, $\gamma = 0$, and the system is in the critical phase where all states are critical. Furthermore, in the localized phase, by expanding the LE around phase transition points, we get $\gamma \propto |V/W - 1|^{1/2}$ when $W > t/\cosh(h)$. In contrast to the critical exponent 1 of the classic AAH model, the critical exponent 1/2 is different. This implies that when $W > t/\cosh(h)$ the system belongs to an unusual

universality class, which was also observed in the AAH model with unbounded quasiperiodic potentials [83]. When $W < t/\cosh(h)$ the system is in the same universality class as for the classic AAH model, given that $\gamma \propto |V/t - 1|^1$ when $W < t/\cosh(h)$.

The above analytical results agree well with numerical simulations. To validate the theoretically computed LE in Eq. (5), we first fit single-particle eigenstates numerically, using exponential wave functions $\phi_j^k = \exp(-\gamma_k|j - j_0|)$. j_0 denotes the localization center, k is the index of states, and γ_k is the LE of state. Then, mean LE $\gamma = \sum_k \gamma_k/L$ is defined by averaging over all eigenstates, and it is plotted for systems with varied h in Fig. 2(a) and its inset. When $W < t/\cosh(h)$, after subtracting the constant $|h|$, all curves collapse into a single one which is consistent with the theoretical prediction in Eq. (6). While when $W > t/\cosh(h)$, the LEs are independent of the complex phase h and in agreement with the prediction in Eq. (7) [see the inset of Fig. 2(a)]. To delve deeper into localization details and determine phase diagram, we compute inverse of the participation ratios (IPRs) and fractal dimensions of states. The IPR is defined by $P_k = \sum_j |\phi_j^k|^4$ for a normalized single-particle state. Generally, the IPR $P_k \propto L^{-\alpha}$, where α is defined as the fractal dimension. For an extended state, $P_k \propto 1/L$ and $\alpha = 1$, whereas the IPR approaches one and $\alpha = 0$ for a localized state. Critical states with $0 < \alpha < 1$ exhibit multifractal properties. In Fig. 2(b), we present the mean fractal dimension $\text{MFD} = \sum_k \alpha_k/L$ on the (V, W) plane, which is obtained numerically using the box-counting approach [88]. When both

V and W are small the system is in the extended phase with $\text{MFD} = 0$, while it is in the localized (critical) phase when $V(W)$ is sufficiently large. The boundary between extended and critical phases is precisely described by $W = t / \cosh(h)$ [black dashed line in Fig. 2(b)], which moves downwards as $|h|$ grows. The critical-localized phase boundary is described by $V = W$ and independent of $|h|$. Thus, the region of the critical phase enlarges as $|h|$ increases. The boundary between extended and localized phases is described by Eq. (10), which makes the area of the extended phase shrink and the region of the localized phase enlarge when $|h|$ increases.

Now we look into the spectral properties. Typical spectra on the complex energy plane for systems in various phases are displayed in Fig. 2(c). The spectrum is real when the system is in the extended phase. However, it becomes complex with loops when the system is in the critical or localized phase. To investigate the real-complex transition, in Fig. 2(d) we present the logarithm of the largest value of imaginary parts of all eigenenergies $\log_{10}[\max |\text{Im}(E)|]$ on the (V, W) plane. The real-complex phase transition point, where the value changes abruptly, is the same as the localization one (dot lines).

In addition to the real-complex transition, nontrivial topological structures (loops) also can exist in the spectrum. To characterize topology of spectrum, winding numbers were utilized without further explanation, which were defined by [43,53,61,88]

$$\nu_\tau(E_B) = \lim_{L \rightarrow \infty} \frac{1}{2\pi i} \int_0^{2\pi/L} d\tau \frac{\partial}{\partial \tau} \ln[\det(H - E_B)], \quad (11)$$

with $\tau = \theta$ or φ . To coordinate the definition of ν_φ , the phase φ has been introduced in the hopping of H , i.e., $H_0 = \sum_j [t_j(e^{-\eta-i\varphi} c_{j+1}^\dagger + e^{\eta+i\varphi} c_{j+1}^\dagger c_j)]$. They characterize how the complex spectral trajectory E encircles a base energy E_B on the complex energy plane when τ goes from 0 to $2\pi/L$. Actually, in the terminology of the 2D model, φ and θ represent momenta in the x and y dimensions, respectively. Consequently, ν_φ and ν_θ characterize the spectral topologies of the 2D model in the x and y dimensions, respectively. For AAH models, the most nontrivial winding numbers for any E_B , i.e., $\nu_\tau = \text{sgn}[\nu_\tau(E_B)] \cdot \max(|\nu_\tau(E_B)|)$, $\forall E_B \in \mathbb{C}$, are usually utilized to characterize the presence of loops on the complex energy plane [53,61,88]. In (the inset of) Fig. 2(e) we show the winding number ν_θ versus V (W), while ν_φ is always zero because we have set $\eta = 0$ in this section. Topological phase transition points are also the same as the localization ones [dash lines in Fig. 2(e)]. The winding number ν_θ in various phases is presented in Fig. 2(b).

Now we explain why the winding number ν_θ , defined by integrating over θ or in the y dimension, can characterize the presence of loops for the 1D AAH model with a fixed θ . Same as in the non-Bloch band theory, the non-Hermiticity h complexes the global phase θ or the momentum in the y dimension and results in loops and nontrivial topology in the y dimension. Furthermore, in the thermodynamic limit, for the 1D AAH model the spectrum is independent of the global phase θ . Correspondingly, for the 2D model the spectrum is independent of the momentum in the y dimension, when PBC is used. The nontrivial spectral topology in the y dimension means that for the 2D model, the complex spectral trajectory E for a fixed momentum in the y dimension forms loops on the

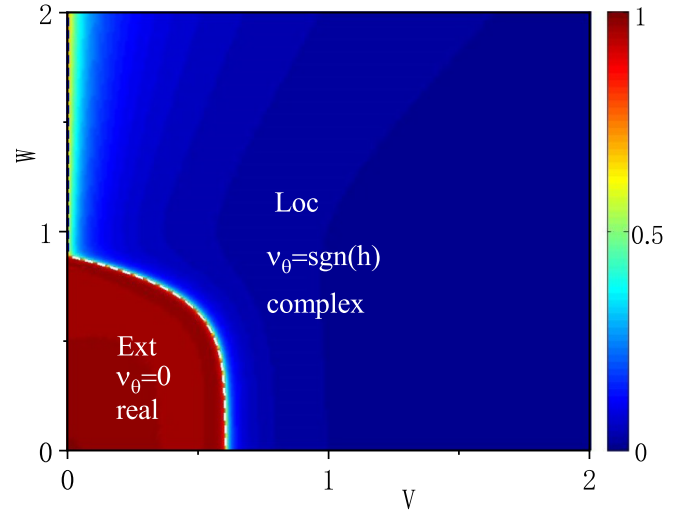


FIG. 3. Mean fractal dimension on the (V, W) plane, of the generalized AAH model in the absence of nonreciprocal hopping ($\eta = 0$), under the periodic boundary condition, and with $\delta = \pi/5$, $h = 0.5$, and $L = 610$.

energy plane. Moreover, the loops spin when the momentum in the y dimension increases. After the dimension reduction, the nontrivial winding number ν_θ results in loops in the spectrum of the 1D AAH model, which spin clockwise (positive h) or counterclockwise (negative h) as θ increases [see Fig. 2(f)]. When h is the lone source of the nontrivial topology, as is the case here, the winding number faithfully represents the presence of loops in the spectrum. Moreover, in the 2D model, the nontrivial winding number ν_θ can result in y -boundary-dependent spectra and skin effect when OBC is used in the y dimension. However, when performing dimension reduction only PBC is used in the y dimension. The open boundary for the 1D AAH model corresponds to the open boundary in the x dimension for the 2D model. The winding number ν_θ in the y dimension cannot cause x -boundary-dependent spectra and the skin effect in the x dimension. Thus, the 1D AAH model with only nonzero h lacks boundary-dependent spectra and skin effect, despite the presence of loops and nontrivial winding number ν_θ .

B. Case $\delta \neq 0$

When $\delta \neq 0$, the numerical mean LEs continue to match the theoretical prediction in Eq. (5) (not shown). Here in Fig. 3 we only provide an exemplary mean fractal dimension on the (V, W) plane. When both V and W are small the system is in the extended phase. It is in the localized phase elsewhere, with the exception of the case that $V = 0$ and $W > t / \cosh(h)$. The boundary between extended and localized phases is described by Eq. (8) (white dashed line), which moves to the origin and shrinks the extended phase as $|h|$ increases. Only when $V = 0$ and $W > t / \cosh(h)$, or at the aforementioned phase boundary, do critical states exist.

As for the spectrum, the real-complex and topological transitions are in accordance with the localization one. When the system is in the extended phase, the spectrum is completely real with zero winding number ν_θ . It is complex, with loops

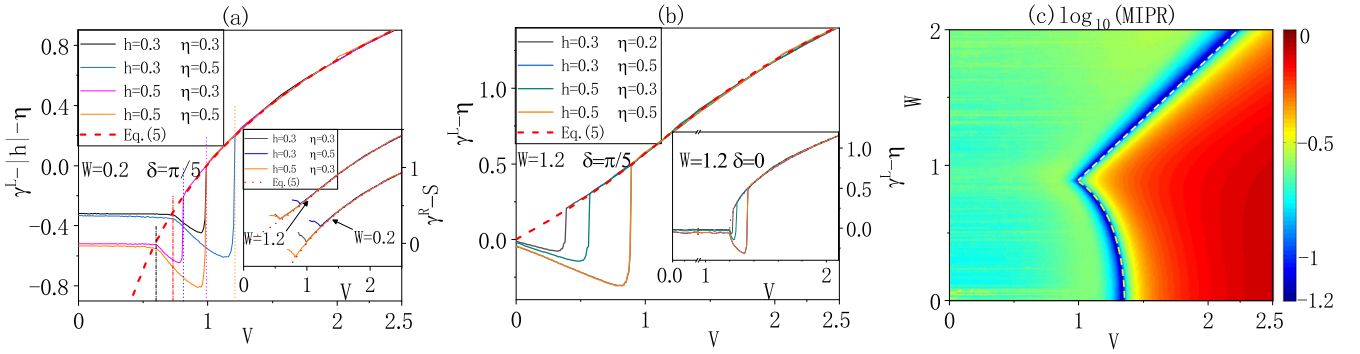


FIG. 4. Generalized AAH model with nonreciprocal hopping ($\eta \neq 0$) and under the open boundary condition. In (a) and its inset we present the shifted mean left- and right-side LEs, respectively, for systems with $\delta = \pi/5$ and various h , η , and W . The constant $S = -\eta$ when $W > t/\cosh(h)$, and $S = |h| - \eta$ when $W < t/\cosh(h)$. Shifted mean left-side LEs versus V are illustrated in (b) and its inset, for systems with $W > t/\cosh(h)$ and different δ . (c) The quantity $\log_{10}(\text{MIPR})$ on the (V, W) plane for the system with $h = 0.5$, $\eta = 0.8$, and $\delta = \pi/5$. The size of lattice is $L = 233$.

and nontrivial ν_θ , when the system is in the localized phase. On critical lines there are two distinct situations. At the boundary between extended and localized phases the spectrum is real and loop-free, while when $V = 0$ and $W > t/\cosh(h)$ [black dashed line in Fig. 3] the spectrum is complex with loops. The winding number ν_θ on the black dashed line is the same as in the localized phase, where spectral loops spin clockwise (positive h) or counterclockwise (negative h) as θ increases. The other winding number ν_φ is always zero because $\eta = 0$.

IV. EFFECTS OF NONRECIPROCAL HOPPING ($\eta \neq 0$)

When η is nonzero, the 2D model has nonreciprocal hoppings in the x dimension (the remaining dimension after reduction) and can have nontrivial spectral topology in this dimension. Therefore, the AAH model supports the non-Hermitian skin effect under OBC and has spectra and states that are boundary dependent. Let us first focus on the scenario under OBC, where localization properties can be analytically determined by using a similarity transformation. Under OBC, the Hamiltonian in Eq. (1) can be transformed into $H_1 = \sum_j [t_j(\tilde{a}_j a_{j+1} + \tilde{a}_{j+1} a_j) + V_j \tilde{a}_j a_j]$ by the asymmetric similarity transformation $c_j = e^{\eta j} a_j$ and $c_j^\dagger = e^{-\eta j} \tilde{a}_j$. The annihilation (creation) operator a_j (\tilde{a}_j) satisfies

$[a_j, \tilde{a}_{j'}]_\pm = \delta_{jj'}$. However, \tilde{a}_j is not the Hermitian conjugate of a_j due to the presence of η . The spectrum and right eigenstates of the Hamiltonian H_1 are identical to those of the Hamiltonian $H(\eta = 0)$ without the nonreciprocal hopping. Therefore, Hamiltonians H and $H(\eta = 0)$ have the same spectra and winding numbers under OBC.

Through the asymmetric similarity transformation, a relationship between single-particle states also can be established. If ϕ_j^k is a right eigenstate of H_1 , then $\psi_j^k = e^{\eta j} \phi_j^k$ is an eigenstate of H [70]. For extended and critical eigenstates of H_1 , corresponding wave functions ψ_j^k are exponentially localized at the right end with left-side LEs $\gamma^L = \eta$ when $\eta > 0$ or at the left end with right-side LEs $\gamma^R = -\eta$ when $\eta < 0$. In contrast, for localized bulk eigenstates of H_1 , corresponding wave functions $\psi_j^k \propto \exp[-(\gamma - \eta)(j - j_0)]$ when $j > j_0$ and $\psi_j^k \propto \exp[-(\gamma + \eta)(j_0 - j)]$ when $j < j_0$, with γ in Eq. (5). Consequently, in the localized phase, bulk states are asymmetrically localized with right- and left-side LEs $\gamma^{R/L} = \gamma \mp \eta$. Evidently, $\gamma - |\eta| > 0$ suggests that all eigenstates are localized in the bulk, whereas $\gamma - |\eta| < 0$ implies that the system is in the skin phase where all eigenstates are localized at one end. Localization phase transition points are determined by $\gamma - |\eta| = 0$. Inserting Eqs. (5)–(7), the condition for localization phase transition is obtained:

$$\frac{V^2 \cos^2 \delta}{[t \cosh(|\eta| - |h|) + \sqrt{t^2 - W^2} \sinh(|\eta| - |h|)]^2} + \frac{V^2 \sin^2 \delta}{(t \sinh(|\eta| - |h|) + \sqrt{t^2 - W^2} \cosh(|\eta| - |h|))^2} = 1, \quad \text{when } W \leq t/\cosh(h), \quad (12)$$

$$\frac{V^2}{W^2} \left[\frac{\cos^2 \delta}{\cosh^2 |\eta|} + \frac{\sin^2 \delta}{\sinh^2 |\eta|} \right] = 1, \quad \text{when } W > t/\cosh(h). \quad (13)$$

The localization remains unaffected by h when $W > t/\cosh(h)$.

Numerical verification of the above analytical results under OBC is in order. In Fig. 4(a) and its inset, we present typical numerical mean left- and right-side LEs versus V

when $W \leq t/\cosh(h)$, respectively. When V is small, all bulk states are localized at one end, implying that the system is in the skin phase [53,70]. As examples, we used positive η , and states are localized at the right end, with $\gamma^L = \eta$ and undefined γ^R . When V is sufficiently large, the system enters

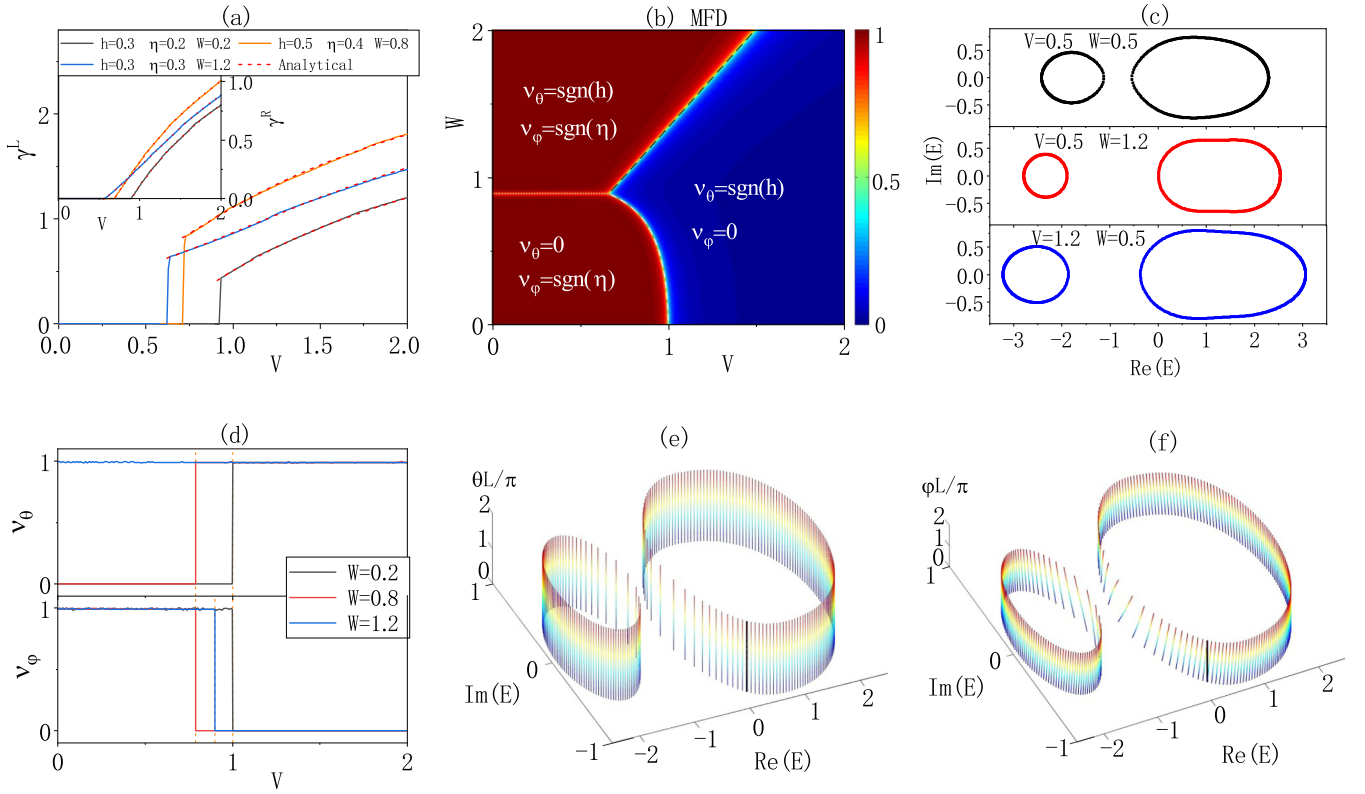


FIG. 5. Generalized AAH model with nonreciprocal hopping ($\eta \neq 0$) and under the periodic boundary condition. In (a) and its inset we present mean left- and right-side LEs versus V respectively, for systems with $\delta = \pi/5$ and various h, η , and W . Dot lines are corresponding analytical LEs, obtained from Eqs. (5)–(7) and the asymmetric similarity transformation. (b) Mean fractal dimension on the (V, W) plane. (c) Typical spectra on the energy plane. (d) Winding numbers ν_θ and ν_ϕ versus V . In (e) and (f) we present how the loops in the first panel of (c) spin as θ and ϕ increase from 0 to $2\pi/L$, respectively. The system is in the lower extended phase. In (b)–(f), systems are with $h = 0.5$, $\eta = 0.5$, and $\delta = \pi/5$. The size of lattice is $L = 610$ in (a)–(d) and $L = 233$ in (e) and (f).

the localized phase. States are asymmetrically localized in the bulk with $\gamma^L = \gamma^R + 2\eta$. Furthermore, after shifting, all LEs in the localized phase collapse into a single curve that matches the theoretical prediction (dot lines). Phase transition points, where γ^L jump abruptly, are in line with Eq. (12) (dash lines). The system is still in the skin phase just before the transition, albeit with a decreasing γ^L . Delocalization of states occurs as V grows. The delocalization begins at the transition point of the corresponding system with $\eta = 0$ [Eq. (8) and dash-dot lines] and ends at the transition point for finite η [Eq. (12) and dash lines]. This is exactly what the asymmetric similarity transformation induces [70]. When $W > t/\cosh(h)$, the localization is the same as above, with the exception that when $\delta \neq 0$ the system in the skin phase is always delocalizing because the transition point lies at $V = 0$ when $\eta = 0$ [see Fig. 4(b)]. Furthermore, in Fig. 4(c) we display a typical $\log_{10}(\text{MIPR})$ on the (V, W) plane. The mean inverse of participation ratio $\text{MIPR} = \sum_k P_k/L$ approaches one in both the skin and localized phases. States in both phases are localized but with different localization details. Phase transition points correspond to the most extended situations with the lowest MIPRs, which comply with the condition in Eqs. (12) and (13) (dash lines).

Under PBC, the asymmetric similarity transformation is no longer effective, and the system has altered spectral and state properties. We first present typical numerical mean left- and

right-side LEs in Fig. 5(a) and its inset. When V is small, the LEs are zero, and the system is in the extended or critical phase. In contrast, for a large-enough V it is in the localized phase, where states are asymmetrically localized with different $\gamma^{R/L}$. The LEs agree with the theoretical prediction $\gamma^{R/L} = \gamma \mp \eta$ obtained under OBC (dash lines), indicating that the localization is independent of boundary conditions when the system is in the localized phase. At transition points [Eqs. (12) and (13) and dot lines], an abrupt jump of size 2η in the mean left-side LE occurs.

To further determine the existence of the critical phase and structure of the localization phase diagram we exhibit a typical MFD on the (V, W) plane in Fig. 5(b). When both V and W are small the system is in the extended phase. In addition, the system is also in the extended phase when V is small but W is large enough. Once the nonreciprocal hopping is introduced, the critical phase at $\delta = 0$ disappears and the extended phase emerges regardless of δ . These two extended phases are separated by a critical line which is described by the equation $W = t/\cosh(h)$ (white dotted line). The line is η independent and moves downwards as $|h|$ increases. When V is sufficiently large the system enters the asymmetrically localized phase. The boundary between the upper extended phase and the localized phase is described by Eq. (13), which is a straight line passing through the origin. The line's slope is independent of h , increases from $\cosh^{-1}(\eta)$ to $\sinh^{-1}(|\eta|)$

when δ increases from 0 to $\pi/2$, and decreases as $|\eta|$ increases. Therefore, the tricritical point moves to the origin as $|h|$ increases, moves left along the horizontal critical line as δ increases, and moves right as $|\eta|$ increases. The boundary between the lower extended phase and the localized phase is described by Eq. (12), which links the tricritical point to the δ -independent transition point ($V = te^{|\eta|-|h|}$, $W = 0$) [53]. From above, we observe that as $|h|$ increases the area of the lower extended phase shrinks while areas of the other two phases expand, and as $|\eta|$ increases areas of both extended phases enlarge while the area of the localized phase shrinks.

On the spectral side, in Fig. 5(c) we present typical spectra in different phases for systems under PBC. As long as parameters are finite, they are complex and always have loops, even on critical lines. Furthermore, we show winding numbers ν_θ and ν_φ versus V in Fig. 5(d). The topological phase transition points are the same as the localization ones, and we present winding numbers in different phases in Fig. 5(b). When both h and η are finite, loops can have two topological origins. The 2D model has nonreciprocal hoppings in both the reduced y and the remaining x dimensions. Spectral topologies in both dimensions can be nontrivial and are determined by the interplay of nonreciprocal hoppings. In the lower extended phase, the nonreciprocal hopping in the remaining x dimension prevails, $\nu_\theta = 0$, and ν_φ is nontrivial. The spectral topology is trivial in the reduced y dimension and nontrivial in the remaining x dimension, which results in the skin effect under x -OBC. Furthermore, the spectrum of the AAH model is still independent of phases θ and φ in the thermodynamic limit. $\nu_\theta = 0$ indicates that the spectrum does not spin as θ increases [see Fig. 5(e)]. In contrast, it spins clockwise (positive η) or counterclockwise (negative η) as φ increases, when ν_φ is nontrivial [see Fig. 5(f)]. It means that in the lower extended phase, the presence of loops in spectrum is because of the spectral topology or the prevailed nonreciprocal hopping in the remaining x dimension. In the localized phase, ν_θ is nontrivial and $\nu_\varphi = 0$ indicates the suppression of the skin effect. The spectral topology is only nontrivial in the reduced y dimension. The spectrum only spins when θ varies, like in Fig. 2(f). Loops exist because of the spectral topology or the prevailed nonreciprocal hopping in the reduced y dimension. However, in the upper extended phase, both winding numbers are nontrivial, and the spectral topologies are nontrivial in both dimensions. The spectral topologies in different dimensions are not mutually exclusive. The spectrum spins both when θ and φ vary separately, and loops originate from nonreciprocal hoppings in both dimensions.

V. CONCLUSION

We have investigated localization and topological properties of generalized AAH models with both on-site and

off-diagonal modulations. The model is the dimension reduction of the 2D non-Hermitian Hall model with nonreciprocal hoppings in both dimensions and the next-nearest-neighbor hopping. Non-Hermiticity arises in the AAH model from the nonreciprocal hopping and the complex global phase. Applying Avila's global theory, we first analytically computed the LE of single-particle eigenstates for systems without nonreciprocal hopping. Based on it, phase diagrams were determined, and analyses of localization properties were conducted. The localization crucially depends on the relative phase between on-site and off-diagonal modulations. The complex global phase is in favor of the critical phase, whose transition to the localized phase falls outside the universality class for the classic AAH model. The real-complex and topological transitions of the spectrum are consistent with the localization one. By mapping to the 2D non-Hermitian Hall model, we clearly explain the physical origin of the spectral topology through winding numbers in different dimensions.

In the presence of nonreciprocal hopping, the model supports the skin effect and has boundary-dependent spectra and states. Under OBC, the localization was analytically studied by employing a similarity transformation, and phase diagrams were precisely determined. As the strength of potential increases, the system turns from the skin phase into the asymmetrically localized phase. When the boundary condition shifts from open to periodic, the skin phase splits into two extended phases separated by a critical line, while the localized phase remains unchanged. Nonreciprocal hopping eliminates the critical phase. The spectrum is always complex and has loops that have distinct topological origins in different phases.

ACKNOWLEDGMENTS

This work is supported by the Innovation Program for Quantum Science and Technology under Grant No. 2023ZD0300400, the Natural Science Foundation of Hubei Province under Grant No. 2022CFB272, and the National Natural Science Foundation of China under Grants No. 12134015 and No. 12175290.

APPENDIX A: DIMENSION REDUCTION

In the Landau gauge $\mathbf{A} = (0, \beta n)$, the 2D model is described by the Hamiltonian in Eq. (3). Let β be approximated by the rational number $\beta \simeq M/L$ and the size of the 2D lattice is $L \times L$. For simplicity, we further utilize periodic boundary conditions in x and y dimensions. The 2D model has translational symmetry in the y dimension. After performing the Fourier transformation in this dimension, we obtain

$$H = \sum_{n,k_y} \left\{ \left(t + W \cos \left[2\pi \frac{M}{L} (n + 1/2) - ih + k_y \right] \right) (e^{-\eta} c_{n,k_y}^\dagger c_{n+1,k_y} + e^\eta c_{n+1,k_y}^\dagger c_{n,k_y}) + 2V \cos \left(2\pi \frac{M}{L} n - ih + \delta + k_y \right) c_{n,k_y}^\dagger c_{n,k_y} \right\}, \quad (\text{A1})$$

where $k_y = \frac{k}{L}2\pi$ and $n, k = 0, \dots, L-1$. For a fixed k_y , the above Hamiltonian is in the form of the AAH model. Furthermore, when we increase the momentum k_y by $2\pi/L$, the Hamiltonian remains the same, by shifting the lattice index n to $n + n_0$ so that $\text{mod}(Mn_0, L) = L-1$ and emerging phases in cosine functions cancel. Then, properties, such as spectrum and localization lengths of eigenstates, of the AAH model are independent of the momentum k_y , and people usually omit k_y . However, detailed information about states like localization centers does depend on k_y . We omit the dependence of k_y in operators, replace k_y with θ , and obtain

$$H^x(\theta) = \sum_n \{(t + W \cos[2\pi\beta(n + 1/2) - ih + \theta])(e^{-\eta}c_n^\dagger c_{n+1} + e^\eta c_{n+1}^\dagger c_n) + 2V \cos(2\pi\beta n - ih + \delta + \theta)c_n^\dagger c_n\}, \quad (\text{A2})$$

which is precisely the non-Hermitian AAH model in Eq. (1).

On the other side, we employ another gauge $\mathbf{A} = (-\beta m, 0)$, and the 2D model is described by the Hamiltonian

$$H_{2D}^2 = \sum_{m,n} t e^{-\eta - i2\pi\beta m} c_{n+1,m}^\dagger c_{n,m} + t e^{-\eta + i2\pi\beta m} c_{n,m}^\dagger c_{n+1,m} + V e^h c_{n,m+1}^\dagger c_{n,m} + V e^{-h} c_{n,m}^\dagger c_{n,m+1} + \frac{W}{2} e^{-i2\pi\beta(m+\frac{1}{2}) + \eta + h - i\delta} c_{n+1,m+1}^\dagger c_{n,m} \\ + \frac{W}{2} e^{i2\pi\beta(m+\frac{1}{2}) - \eta - h + i\delta} c_{n,m}^\dagger c_{n+1,m+1} + \frac{W}{2} e^{-i2\pi\beta(m+\frac{1}{2}) + \eta - h + i\delta} c_{n+1,m}^\dagger c_{n,m+1} + \frac{W}{2} e^{i2\pi\beta(m+\frac{1}{2}) - \eta + h - i\delta} c_{n,m+1}^\dagger c_{n+1,m}. \quad (\text{A3})$$

This Hamiltonian has translational symmetry in the x dimension, and after performing the Fourier transformation in this dimension, we obtain

$$H_{2D}^2 = \sum_{m,k_x} (V e^{-h} c_{m,k_x}^\dagger c_{m+1,k_x} + V e^h c_{m+1,k_x}^\dagger c_{m,k_x}) \\ + \sum_{m,k_x} W \cos[2\pi\beta(m + 1/2) + i\eta - k_x] \\ \times (e^{-h+i\delta} c_{m,k_x}^\dagger c_{m+1,k_x} + e^{h-i\delta} c_{m+1,k_x}^\dagger c_{m,k_x}) \\ + \sum_{m,k_x} 2t \cos(2\pi\beta m + i\eta - k_x) c_{m,k_x}^\dagger c_{m,k_x}. \quad (\text{A4})$$

Omitting the k_x dependence, we have

$$H^y = \sum_m (V e^{-h} c_m^\dagger c_{m+1} + V e^h c_{m+1}^\dagger c_m) \\ + \sum_m W \cos[2\pi\beta(m + 1/2) + i\eta] \\ \times (e^{-h+i\delta} c_m^\dagger c_{m+1} + e^{h-i\delta} c_{m+1}^\dagger c_m) \\ + \sum_m 2t \cos(2\pi\beta m + i\eta) c_m^\dagger c_m. \quad (\text{A5})$$

This is another AAH model which is similar to Eq. (1) or Eq. (A2). When $\delta = 0$ and omitting the θ dependence entirely, H^x and H^y are in the same form, and one can be mapped to the other by simultaneously interchanging $t \leftrightarrow V$ and $\eta \leftrightarrow h$, and conjugating in addition.

APPENDIX B: COMPUTATION OF LYAPUNOV EXPONENT

By factorizing out the shared denominator, we rewrite the transfer matrix in Eq. (4) as a commutative product:

$$T_j = \begin{bmatrix} \frac{E - V_j}{t_j} & -\frac{t_{j-1}}{t_j} \\ 1 & 0 \end{bmatrix} = A_j B_j, \quad (\text{B1})$$

where

$$A_j = \frac{1}{t + W \cos[2\pi\beta(j + 1/2) + \theta - ih]}, \\ B_j = \begin{bmatrix} E - V_j & -t_{j-1} \\ t_j & 0 \end{bmatrix}. \quad (\text{B2})$$

According to Eqs. (2), t_j and V_j denote the modulated off-diagonal hopping amplitude and on-site complex potential, respectively. The LE of state is computed by

$$\gamma(E) = \lim_{L \rightarrow \infty} \frac{1}{L} \ln \left\| \prod_{j=1}^L T_j \right\|, \\ = \lim_{L \rightarrow \infty} \frac{1}{L} \ln \left\| \prod_{j=1}^L A_j \right\| + \lim_{L \rightarrow \infty} \frac{1}{L} \ln \left\| \prod_{j=1}^L B_j \right\|, \\ = \gamma^A(E) + \gamma^B(E), \quad (\text{B3})$$

where $\|\cdot\|$ represents a matrix's norm, which is defined by the largest absolute value of its eigenvalues. Using Ergodic theory and Jensen's formula [94], we derive

$$\gamma^A(E) = \lim_{L \rightarrow \infty} \frac{1}{L} \ln \prod_{j=1}^L \frac{1}{|t + W \cos[2\pi\beta(j + 1/2) + \theta - ih]|}, \\ = \frac{1}{2\pi} \int_0^{2\pi} \ln \frac{1}{|t + W \cos(\theta - ih)|} d\theta, \\ = \begin{cases} \ln \frac{2}{t + \sqrt{t^2 - W^2}}, & W \leq t / \cosh(h), \\ \ln \frac{2}{W} - |h|, & W > t / \cosh(h). \end{cases} \quad (\text{B4})$$

Regarding $\gamma^B(E)$, we apply Avila's global theory. First, we need to make an analytical continuation of the global phase, i.e., $\theta \rightarrow \theta + i\varepsilon$. We will use the same symbol to represent a quantity before and after its analytical continuation if there is no room for confusion. In the limit $\varepsilon \rightarrow +\infty$, we easily attain

$$B_j(\varepsilon \rightarrow +\infty) \\ = e^{-i2\pi\beta j + \varepsilon - h} \begin{bmatrix} -V e^{-i\delta} & -W e^{i\pi\beta/2} \\ W e^{-i\pi\beta/2} & 0 \end{bmatrix} + o(1), \quad (\text{B5})$$

resulting in

$$\gamma_{\varepsilon \rightarrow +\infty}^B(E) = \varepsilon - h + \max \left\{ \ln \frac{|Ve^{-i\delta} \pm \sqrt{[Ve^{-i\delta}]^2 - W^2}|}{2} \right\}. \quad (\text{B6})$$

On the other side, in the limit $\varepsilon \rightarrow -\infty$, a direct computation yields

$$B_j(\varepsilon \rightarrow -\infty) = e^{i2\pi\beta j - \varepsilon + h} \begin{bmatrix} -Ve^{i\delta} & -We^{-i\pi\beta/2} \\ We^{i\pi\beta/2} & 0 \end{bmatrix} + o(1), \quad (\text{B7})$$

and the corresponding LE is

$$\gamma_{\varepsilon \rightarrow -\infty}^B(E) = |\varepsilon| + h + \max \left\{ \ln \frac{|Ve^{i\delta} \pm \sqrt{[Ve^{i\delta}]^2 - W^2}|}{2} \right\}. \quad (\text{B8})$$

According to Avila's global theory, as a function of ε , $\gamma_\varepsilon^B(E)$ is a convex, piecewise linear function with integer slopes. Moreover, the theory shows that, the energy E does not belong to the spectrum, if and only if $\gamma_{\varepsilon=0}^B(E) > 0$ and $\gamma_\varepsilon^B(E)$ is an

affine function in the vicinity of $\varepsilon = 0$. Including $\gamma^A(E)$, we obtain the LE of the single-particle state

$$\gamma(E) = \begin{cases} \max(f_1, 0), & W \leq t / \cosh(h), \\ \max(f_2, 0), & W > t / \cosh(h), \end{cases} \quad (\text{B9})$$

where

$$f_1 = \max \left\{ |h| + \ln \frac{|Ve^{i\delta} \pm \sqrt{[Ve^{i\delta}]^2 - W^2}|}{t + \sqrt{t^2 - W^2}} \right\},$$

$$f_2 = \max \left\{ \ln \frac{|Ve^{i\delta} \pm \sqrt{[Ve^{i\delta}]^2 - W^2}|}{W} \right\}. \quad (\text{B10})$$

Quantities $f_{1,2}$ are periodic functions of the relative phase δ with a period π , and are also symmetric with respect to $\delta = m\pi/2$, $m \in \mathbb{Z}$. Consequently, we restrict $\delta \in [0, \pi/2]$. When $\delta \in [0, \pi/2]$, $f_{1,2}$ reduce to

$$f_1 = |h| + \ln \frac{|Ve^{i\delta} + \sqrt{[Ve^{i\delta}]^2 - W^2}|}{t + \sqrt{t^2 - W^2}},$$

$$f_2 = \ln \frac{|Ve^{i\delta} + \sqrt{[Ve^{i\delta}]^2 - W^2}|}{W}, \quad (\text{B11})$$

which are exactly the Eqs. (6) and (7).

-
- [1] P. G. Harper, Single band motion of conduction electrons in a uniform magnetic field, *Proc. Phys. Soc. Lond. Sect. A* **68**, 874 (1955).
 - [2] S. Aubry and G. André, Analyticity breaking and Anderson localization in incommensurate lattices, *Ann. Isr. Phys. Soc.* **3**, 133 (1980).
 - [3] D. R. Hofstadter, Energy levels and wave functions of Bloch electrons in rational and irrational magnetic fields, *Phys. Rev. B* **14**, 2239 (1976).
 - [4] Y. E. Kraus, Y. Lahini, Z. Ringel, M. Verbin, and O. Zilberberg, Topological states and adiabatic pumping in quasicrystals, *Phys. Rev. Lett.* **109**, 106402 (2012).
 - [5] L. J. Lang, X. Cai, and S. Chen, Edge states and topological phases in one-dimensional optical superlattices, *Phys. Rev. Lett.* **108**, 220401 (2012).
 - [6] S. Ganeshan, K. Sun, and S. Das Sarma, Topological zero-energy modes in gapless commensurate Aubry-André-Harper models, *Phys. Rev. Lett.* **110**, 180403 (2013).
 - [7] S. Y. Jitomirskaya, Metal-insulator transition for the almost Mathieu operator, *Ann. Math.* **150**, 1159 (1999).
 - [8] F. Evers and A. D. Mirlin, Anderson transitions, *Rev. Mod. Phys.* **80**, 1355 (2008).
 - [9] S. Das Sarma, S. He, and X. C. Xie, Mobility edge in a model one-dimensional potential, *Phys. Rev. Lett.* **61**, 2144 (1988).
 - [10] X. Cai, L. J. Lang, S. Chen, and Y. Wang, Topological superconductor to Anderson localization transition in one-dimensional incommensurate lattices, *Phys. Rev. Lett.* **110**, 176403 (2013).
 - [11] M. Rossignolo and L. Dell'Anna, Localization transitions and mobility edges in coupled Aubry-André chains, *Phys. Rev. B* **99**, 054211 (2019).
 - [12] X. Deng, S. Ray, S. Sinha, G. V. Shlyapnikov, and L. Santos, One-dimensional quasicrystals with power-law hopping, *Phys. Rev. Lett.* **123**, 025301 (2019).
 - [13] S. Roy, T. Mishra, B. Tanatar, and S. Basu, Reentrant localization transition in a quasiperiodic chain, *Phys. Rev. Lett.* **126**, 106803 (2021).
 - [14] Y. Wang, X. Xia, L. Zhang, H. Yao, S. Chen, J. You, Q. Zhou, and X.-J. Liu, One-dimensional quasiperiodic mosaic lattice with exact mobility edges, *Phys. Rev. Lett.* **125**, 196604 (2020).
 - [15] J. Biddle and S. Das Sarma, Predicted mobility edges in one-dimensional incommensurate optical lattices: An exactly solvable model of Anderson localization, *Phys. Rev. Lett.* **104**, 070601 (2010).
 - [16] S. Ganeshan, J. H. Pixley, and S. Das Sarma, Nearest neighbor tight binding models with an exact mobility edge in one dimension, *Phys. Rev. Lett.* **114**, 146601 (2015).
 - [17] F. A. An, K. Padavić, E. J. Meier, S. Hegde, S. Ganeshan, J. H. Pixley, S. Vishveshwara, and B. Gadway, Interactions and mobility edges: Observing the generalized Aubry-André model, *Phys. Rev. Lett.* **126**, 040603 (2021).
 - [18] T. Liu, S. Cheng, R. Zhang, R. Ruan, and H. Jiang, Invariable mobility edge in a quasiperiodic lattice, *Chin. Phys. B* **31**, 027101 (2022).
 - [19] M. Gonçalves, B. Amorim, E. V. Castro, and P. Ribeiro, Critical phase dualities in 1D exactly solvable quasiperiodic models, *Phys. Rev. Lett.* **131**, 186303 (2023).
 - [20] X.-C. Zhou, Y. Wang, T.-F. J. Poon, Q. Zhou, and X.-J. Liu, Exact new mobility edges between critical and localized states, *Phys. Rev. Lett.* **131**, 176401 (2023).

- [21] D. J. Thouless, Bandwidths for a quasiperiodic tight-binding model, *Phys. Rev. B* **28**, 4272 (1983).
- [22] I. Chang, K. Ikezawa, and M. Kohmoto, Multifractal properties of the wave functions of the square-lattice tight-binding model with next-nearest-neighbor hopping in a magnetic field, *Phys. Rev. B* **55**, 12971 (1997).
- [23] F. Liu, S. Ghosh, and Y. D. Chong, Localization and adiabatic pumping in a generalized Aubry-André-Harper model, *Phys. Rev. B* **91**, 014108 (2015).
- [24] Y. Wang, C. Cheng, X.-J. Liu, and D. Yu, Many-body critical phase: Extended and nonthermal, *Phys. Rev. Lett.* **126**, 080602 (2021).
- [25] G. Roati, C. D'Errico, L. Fallani, M. Fattori, C. Fort, M. Zaccanti, G. Modugno, M. Modugno, and M. Inguscio, Anderson localization of a non-interacting Bose-Einstein condensate, *Nature (London)* **453**, 895 (2008).
- [26] Xiao Li, Xiaopeng Li, and S. Das Sarma, Mobility edges in one-dimensional bichromatic incommensurate potentials, *Phys. Rev. B* **96**, 085119 (2017).
- [27] H. P. Lüschen, S. Scherg, T. Kohlert, M. Schreiber, P. Bordia, X. Li, S. Das Sarma, and I. Bloch, Single-particle mobility edge in a one-dimensional quasiperiodic optical lattice, *Phys. Rev. Lett.* **120**, 160404 (2018).
- [28] T. Kohlert, S. Scherg, X. Li, H. P. Lüschen, S. Das Sarma, I. Bloch, and M. Aidelsburger, Observation of many-body localization in a one-dimensional system with a single-particle mobility edge, *Phys. Rev. Lett.* **122**, 170403 (2019).
- [29] V. Goblot, A. Štrkalj, N. Pernet, J. L. Lado, C. Dorow, A. Lemaître, L. L. Gratiet, A. Harouri, I. Sagnes, S. Ravets, A. Amo, J. Bloch, and O. Zilberberg, Emergence of criticality through a cascade of delocalization transitions in quasiperiodic chains, *Nat. Phys.* **16**, 832 (2020).
- [30] F. A. An, E. J. Meier, and B. Gadway, Engineering a flux-dependent mobility edge in disordered zigzag chains, *Phys. Rev. X* **8**, 031045 (2018).
- [31] Y. Lahini, R. Pugatch, F. Pozzi, M. Sorel, R. Morandotti, N. Davidson, and Y. Silberberg, Observation of a localization transition in quasiperiodic photonic lattices, *Phys. Rev. Lett.* **103**, 013901 (2009).
- [32] J. M. Zeuner, M. C. Rechtsman, Y. Plotnik, Y. Lumer, S. Nolte, M. S. Rudner, M. Segev, and A. Szameit, Observation of a topological transition in the bulk of a non-Hermitian system, *Phys. Rev. Lett.* **115**, 040402 (2015).
- [33] C. Poli, M. Bellec, U. Kuhl, F. Mortessagne, and H. Schomerus, Selective enhancement of topologically induced interface states in a dielectric resonator chain, *Nat. Commun.* **6**, 6710 (2015).
- [34] P. Peng, W. Cao, C. Shen, W. Qu, J. Wen, L. Jiang, and Y. Xiao, Anti-parity-time symmetry with flying atoms, *Nat. Phys.* **12**, 1139 (2016).
- [35] H. Xu, D. Mason, L. Jiang, and J. G. E. Harris, Topological energy transfer in an optomechanical system with exceptional points, *Nature (London)* **537**, 80 (2016).
- [36] S. Weimann, M. Kremer, Y. Plotnik, Y. Lumer, S. Nolte, K. G. Makris, M. Segev, M. C. Rechtsman, and A. Szameit, Topologically protected bound states in photonic parity-time-symmetric crystals, *Nat. Mater.* **16**, 433 (2017).
- [37] M. Pan, H. Zhao, P. Miao, S. Longhi, and L. Feng, Photonic zero mode in a non-Hermitian photonic lattice, *Nat. Commun.* **9**, 1308 (2018).
- [38] H. Zhou, C. Peng, Y. Yoon, C. W. Hsu, K. A. Nelson, L. Fu, J. D. Joannopoulos, M. Soljačić, and B. Zhen, Observation of bulk Fermi arc and polarization half charge from paired exceptional points, *Science* **359**, 1009 (2018).
- [39] C. M. Bender and S. Boettcher, Real spectra in non-Hermitian Hamiltonians having \mathcal{PT} symmetry, *Phys. Rev. Lett.* **80**, 5243 (1998).
- [40] Y. Ashida, Z. Gong, and M. Ueda, Non-Hermitian physics, *Adv. Phys.* **69**, 249 (2020).
- [41] A. Mostafazadeh, Pseudo-Hermitian representation of quantum mechanics, *Int. J. Geom. Methods Mod. Phys.* **07**, 1191 (2010).
- [42] M. Znojil, Unitarity corridors to exceptional points, *Phys. Rev. A* **100**, 032124 (2019).
- [43] Z. Gong, Y. Ashida, K. Kawabata, K. Takasan, S. Higashikawa, and M. Ueda, Topological phases of non-Hermitian systems, *Phys. Rev. X* **8**, 031079 (2018).
- [44] F. Song, S. Yao, and Z. Wang, Non-Hermitian topological invariants in real space, *Phys. Rev. Lett.* **123**, 246801 (2019).
- [45] S. Yao and Z. Wang, Edge states and topological invariants of non-Hermitian systems, *Phys. Rev. Lett.* **121**, 086803 (2018).
- [46] N. Okuma, K. Kawabata, K. Shiozaki, and M. Sato, Topological origin of non-Hermitian skin effects, *Phys. Rev. Lett.* **124**, 086801 (2020).
- [47] T. E. Lee, Anomalous edge state in a non-Hermitian lattice, *Phys. Rev. Lett.* **116**, 133903 (2016).
- [48] D. Leykam, K. Y. Bliokh, C. Huang, Y. D. Chong, and F. Nori, Edge modes, degeneracies, and topological numbers in non-Hermitian systems, *Phys. Rev. Lett.* **118**, 040401 (2017).
- [49] H. Shen, B. Zhen, and L. Fu, Topological band theory for non-Hermitian Hamiltonians, *Phys. Rev. Lett.* **120**, 146402 (2018).
- [50] F. K. Kunst, E. Edvardsson, J. C. Budich, and E. J. Bergholtz, Biorthogonal bulk-boundary correspondence in non-Hermitian systems, *Phys. Rev. Lett.* **121**, 026808 (2018).
- [51] K. Yokomizo and S. Murakami, Non-Bloch band theory of non-Hermitian systems, *Phys. Rev. Lett.* **123**, 066404 (2019).
- [52] D. S. Borgnia, A. J. Kruchkov, and R.-J. Slager, Non-Hermitian boundary modes and topology, *Phys. Rev. Lett.* **124**, 056802 (2020).
- [53] X. Cai, Boundary-dependent self-dualities, winding numbers, and asymmetrical localization in non-Hermitian aperiodic one-dimensional models, *Phys. Rev. B* **103**, 014201 (2021).
- [54] Y. Liu, Q. Zhou, and S. Chen, Localization transition, spectrum structure, and winding numbers for one-dimensional non-Hermitian quasicrystals, *Phys. Rev. B* **104**, 024201 (2021).
- [55] Y. Liu, X.-P. Jiang, J. Cao, and S. Chen, Non-Hermitian mobility edges in one-dimensional quasicrystals with parity-time symmetry, *Phys. Rev. B* **101**, 174205 (2020).
- [56] S. Longhi, \mathcal{PT} -symmetric optical superlattices, *J. Phys. A* **47**, 165302 (2014).
- [57] C. Yuce, \mathcal{PT} symmetric Aubry-Andre model, *Phys. Lett. A* **378**, 2024 (2014).
- [58] C. H. Liang, D. D. Scott, and Y. N. Joglekar, \mathcal{PT} restoration via increased loss and gain in the \mathcal{PT} -symmetric Aubry-André model, *Phys. Rev. A* **89**, 030102(R) (2014).
- [59] A. K. Harter, T. E. Lee, and Y. N. Joglekar, \mathcal{PT} -breaking threshold in spatially asymmetric Aubry-André and Harper models: Hidden symmetry and topological states, *Phys. Rev. A* **93**, 062101 (2016).

- [60] D.-W. Zhang, L.-Z. Tang, L.-J. Lang, H. Yan, and S.-L. Zhu, Non-Hermitian topological Anderson insulators, *Sci. Chin. Phys. Mech. Astron.* **63**, 267062 (2020).
- [61] S. Longhi, Topological phase transition in non-Hermitian quasicrystals, *Phys. Rev. Lett.* **122**, 237601 (2019).
- [62] N. X. A. Rivolta, H. Benisty, and B. Maes, Topological edge modes with \mathcal{PT} symmetry in a quasiperiodic structure, *Phys. Rev. A* **96**, 023864 (2017).
- [63] Q.-B. Zeng, Y.-B. Yang, and Y. Xu, Topological phases in non-Hermitian Aubry-André-Harper models, *Phys. Rev. B* **101**, 020201(R) (2020).
- [64] S. Longhi, Metal-insulator phase transition in a non-Hermitian Aubry-André-Harper model, *Phys. Rev. B* **100**, 125157 (2019).
- [65] Q.-B. Zeng, S. Chen, and R. Lü, Anderson localization in the non-Hermitian Aubry-André-Harper model with physical gain and loss, *Phys. Rev. A* **95**, 062118 (2017).
- [66] A. Jazaeri and I. I. Satija, Localization transition in incommensurate non-Hermitian systems, *Phys. Rev. E* **63**, 036222 (2001).
- [67] S. Longhi, Non-Hermitian topological phase transition in \mathcal{PT} -symmetric mode-locked lasers, *Opt. Lett.* **44**, 1190 (2019).
- [68] Q.-B. Zeng and Y. Xu, Winding numbers and generalized mobility edges in non-Hermitian systems, *Phys. Rev. Res.* **2**, 033052 (2020).
- [69] T. Liu, S. Cheng, H. Guo, and X. Gao, Fate of Majorana zero modes, exact location of critical states, and unconventional real-complex transition in non-Hermitian quasiperiodic lattices, *Phys. Rev. B* **103**, 104203 (2021).
- [70] H. Jiang, L.-J. Lang, C. Yang, S.-L. Zhu, and S. Chen, Interplay of non-Hermitian skin effects and Anderson localization in nonreciprocal quasiperiodic lattices, *Phys. Rev. B* **100**, 054301 (2019).
- [71] S. Longhi, Topological Anderson phase in quasi-periodic waveguide lattices, *Opt. Lett.* **45**, 4036 (2020).
- [72] L. Z. Tang, G. Q. Zhang, L. F. Zhang, and D. W. Zhang, Localization and topological transitions in non-Hermitian quasiperiodic lattices, *Phys. Rev. A* **103**, 033325 (2021).
- [73] T. Liu, H. Guo, Y. Pu, and S. Longhi, Generalized Aubry-André self-duality and mobility edges in non-Hermitian quasiperiodic lattices, *Phys. Rev. B* **102**, 024205 (2020).
- [74] Q.-B. Zeng and R. Lü, Real spectra, Anderson localization, and topological phases in one-dimensional quasireciprocal systems, *New J. Phys.* **24**, 043023 (2022).
- [75] W. Han and L. Zhou, Dimerization-induced mobility edges and multiple reentrant localization transitions in non-Hermitian quasicrystals, *Phys. Rev. B* **105**, 054204 (2022).
- [76] A. P. Acharya, A. Chakrabarty, D. K. Sahu, and S. Datta, Localization, \mathcal{PT} symmetry breaking, and topological transitions in non-Hermitian quasicrystals, *Phys. Rev. B* **105**, 014202 (2022).
- [77] L.-M. Chen, Y. Zhou, S. A. Chen, and P. Ye, Quantum entanglement of non-Hermitian quasicrystals, *Phys. Rev. B* **105**, L121115 (2022).
- [78] D. Peng, S. Cheng, and G. Xianlong, Power-law hopping of single particles in one-dimensional non-Hermitian quasicrystals, *Phys. Rev. B* **107**, 174205 (2023).
- [79] L. Zhou, Non-Abelian generalization of non-Hermitian quasicrystals: \mathcal{PT} -symmetry breaking, localization, entanglement, and topological transitions, *Phys. Rev. B* **108**, 014202 (2023).
- [80] S. Longhi, Phase transitions and bunching of correlated particles in a non-Hermitian quasicrystal, *Phys. Rev. B* **108**, 075121 (2023).
- [81] A. Padhan, S. R. Padhi, and T. Mishra, Complete delocalization and reentrant topological transition in a non-Hermitian quasiperiodic lattice, *Phys. Rev. B* **109**, L020203 (2024).
- [82] A. P. Acharya and S. Datta, Localization transitions in a non-Hermitian quasiperiodic lattice, *Phys. Rev. B* **109**, 024203 (2024).
- [83] Y.-C. Zhang and Y.-Y. Zhang, Lyapunov exponent, mobility edges, and critical region in the generalized Aubry-André model with an unbounded quasiperiodic potential, *Phys. Rev. B* **105**, 174206 (2022).
- [84] X. Cai, Localization and topological phase transitions in non-Hermitian Aubry-André-Harper models with p -wave pairing, *Phys. Rev. B* **103**, 214202 (2021).
- [85] S. Weidemann, M. Kremer, S. Longhi, and A. Szameit, Topological triple phase transition in non-Hermitian Floquet quasicrystals, *Nature (London)* **601**, 354 (2022).
- [86] Q. Lin, T. Li, L. Xiao, K. Wang, W. Yi, and P. Xue, Topological phase transitions and mobility edges in non-Hermitian quasicrystals, *Phys. Rev. Lett.* **129**, 113601 (2022).
- [87] Y. Liu, Y. Wang, X.-J. Liu, Q. Zhou, and S. Chen, Exact mobility edges, \mathcal{PT} -symmetry breaking, and skin effect in one-dimensional non-Hermitian quasicrystals, *Phys. Rev. B* **103**, 014203 (2021).
- [88] X. Cai and S.-J. Jiang, Equivalence and superposition of real and imaginary quasiperiodicities, *New J. Phys.* **24**, 113001 (2022).
- [89] X. Xia, K. Huang, S. Wang, and X. Li, Exact mobility edges in the non-Hermitian t_1 - t_2 model: Theory and possible experimental realizations, *Phys. Rev. B* **105**, 014207 (2022).
- [90] Z. Xu, X. Xia, and S. Chen, Exact mobility edges and topological phase transition in two-dimensional non-Hermitian quasicrystals, *Sci. Chin. Phys. Mech. Astron.* **65**, 227211 (2022).
- [91] Y. Liu, Y. Wang, Z. Zheng, and S. Chen, Exact non-Hermitian mobility edges in one-dimensional quasicrystal lattice with exponentially decaying hopping and its dual lattice, *Phys. Rev. B* **103**, 134208 (2021).
- [92] W. Chen, S. Cheng, J. Lin, R. Asgari, and X. Gao, Breakdown of the correspondence between the real-complex and delocalization-localization transitions in non-Hermitian quasicrystals, *Phys. Rev. B* **106**, 144208 (2022).
- [93] A. Avila, Global theory of one-frequency Schrödinger operators, *Acta Math.* **215**, 1 (2015).
- [94] https://en.wikipedia.org/wiki/Jensen's_formula.